

Cluster and toroidal aspects of isoscalar dipole excitations in ^{12}C

Yoshiko Kanada-En'yo, Yuki Shikata, and Horiyuki Morita
Department of Physics, Kyoto University, Kyoto 606-8502, Japan

We investigated cluster and toroidal aspects of isoscalar dipole excitations in ^{12}C based on the shifted basis antisymmetrized molecular dynamics combined with the generator coordinate method, which can describes 1p-1h excitations and 3α dynamics. In the $E = 10 - 15$ MeV region, we found two low-energy dipole modes separating from the giant dipole resonance. One is the developed 3α -cluster state and the other is the toroidal dipole mode. The cluster state is characterized by the large amplitude cluster motion beyond the 1p-1h model space, whereas the toroidal dipole mode is predominantly described by 1p-1h excitations on the ground state. The low-energy dipole states are remarkably excited by the toroidal dipole operator, which can measure the nuclear vorticity. For compressive dipole transition strengths, a major part is distributed in the $30 - 50$ MeV region for the giant dipole resonance, and 5% of the total energy weighted sum exist in the $E < 20$ MeV region.

I. INTRODUCTION

In these decades, researches of isoscalar monopole (ISM) and dipole (ISD) excitations have been proceeding remarkably through experiments with α inelastic scattering. Recently, particular attention has been paid to low-energy (LE) monopole and dipole strengths below the giant resonances (GR). Since the ISM and ISD operators corresponding to compressive modes can directly excite inter-cluster motions, they are good probes for cluster states as discussed by Yamada *et al.* [1] and Chiba *et al.* [2]. Indeed, in such nuclei as ^{16}O and ^{24}Mg , the LE-ISM and ISD strengths are described by cluster states, which appear separating from the collective modes of the GRs.

In the progress in physics of unstable nuclei, the LE-ISD excitations have been also discussed in relation to isovector (IV) dipole excitations (see, e.g., reviews in Refs. [3–6] and references therein). Owing to experimental studies with hadronic probes, information of isospin characters of the LE dipole (LED) excitations are becoming available for various nuclei. The IS giant dipole resonances (GDR), which correspond to the collective compressive dipole mode, have been observed for stable nuclei in the energy region higher than that of the IVGDR for the proton-neutron opposite oscillation mode. Below the ISGDR, significant LE-ISD strengths have been known in stable nuclei [7–9]. In the ISD strengths of ^{16}O and ^{40}Ca , 4–5% of the energy weighted sum rule have been observed in the $E \leq 10$ MeV region.

In order to understand the LED strengths, the toroidal dipole (TD) mode (called also the torus or vortical mode) has been proposed with hydrodynamical models [10, 11]. The TD mode carries vorticity and its character is much different from the compressive dipole (CD) mode, which corresponds to the ordinary ISD mode contributing to the ISGDR. The energy of the TD mode is expected to be lower than the ISGDR energy because it conserves the nuclear density. In these years, microscopic calculations with quasiparticle phonon model (QPM) and random phase approximation (RPA) have been achieved, and toroidal natures of the LED excitations in various

nuclei have been investigated [3, 12–17].

In the ISD strengtsh of ^{12}C measured by α inelastic scattering, several percentages of the energy weighted sum rule have been observed in the $E \leq 20$ MeV region below the ISGDR energy [18]. In the LE-ISD strengths, there is a peak for the 1_1^- state at 10.8 MeV. In addition, another peak (or bump) structure around 15 MeV exists indicating a possible existence of the LED mode other than the 1^- (10.8 MeV). In theoretical studies of ^{12}C , a variety of 3α -cluster states have been suggested in excited states above the 3α threshold energy (7.16 MeV). Microscopic 3α -cluster models [19–22] describe a spatially developed 3α -cluster structure of the 1_1^- state. Even though cluster models are useful for 3α -cluster states of ^{12}C , the models *a priori* assume three α clusters, and therefore they are insufficient to study 1p-1h excitations and unable to describe GRs. In order to take into account coherent 1p-1h excitations for the GRs as well as the large amplitude cluster modes, one of the authors, Y. K-E., has extended the antisymmetrized molecular dynamics (AMD) [23–26] and constructed a new method, the shifted basis AMD combined with the generator coordinate method (GCM) with respect to the inter-cluster motion, which we named “sAMD+GCM” [27–29]. In the previous work [29], we applied the sAMD+GCM to calculate ISM and ISD transition strengths of ^{12}C and obtained significant LE-ISD strengths in the $E = 10 - 15$ MeV region well separating from the high-energy strengths for the ISGDR.

Our aim in this paper is to clarify natures of the LE-ISD excitations of ^{12}C , in particular, cluster and toroidal aspects, by reanalysis of the previous calculation. To probe the toroidal nature, we adopt the TD operator in addition to the CD operator for the ordinary ISD and show the remarkable TD strengths for two LE-ISD modes, the 1_1^- with the developed 3α -cluster structure and the 1_2^- dominated by 1p-1h configurations with significant cluster breaking. We also discuss the TD mode from a cluster picture and its connection with 1p-1h excitations in a shell-model limit.

The paper is organized as follows. The framework of the sAMD+GCM for ^{12}C is explained in Sec. II. Defini-

tions of ISD operators are given in Sec. III. Section IV shows the calculated results and discusses properties of the LED modes. The intrinsic structure of the TD mode and its shell-model limit are presented in Sec. VI. Finally, the paper concludes with a summary and an outlook in section VII.

II. SAMD+GCM

The sAMD+GCM has been applied to ISM, ISD, and $E1$ excitations of light nuclei such as ^{10}Be , ^{12}C and ^{16}O [27–29]. A similar method has been recently applied to $E1$ and ISD excitations of ^{26}Ne by Kimura [30]. In the previous work, we applied the sAMD+GCM to ^{12}C by taking into account 3α -cluster configurations. For the detailed procedure of the sAMD+GCM calculation, the reader is referred to Ref. [29].

In the AMD method, a basis wave function is given by a Slater determinant,

$$\Phi_{\text{AMD}}(\mathbf{Z}) = \frac{1}{\sqrt{A!}} \mathcal{A}\{\varphi_1, \varphi_2, \dots, \varphi_A\}, \quad (1)$$

where \mathcal{A} is the antisymmetrizer, and φ_i is the i th single-particle wave function written by a product of spatial, spin, and isospin wave functions,

$$\varphi_i = \phi_{\mathbf{X}_i} \chi_i \tau_i, \quad (2)$$

$$\phi_{\mathbf{X}_i}(\mathbf{r}_j) = \left(\frac{2\nu}{\pi}\right)^{3/4} \exp[-\nu(\mathbf{r}_j - \mathbf{X}_i)^2], \quad (3)$$

$$\chi_i = \left(\frac{1}{2} + \xi_i\right)\chi_{\uparrow} + \left(\frac{1}{2} - \xi_i\right)\chi_{\downarrow}, \quad (4)$$

where $\phi_{\mathbf{X}_i}$ and χ_i are the spatial and spin functions, respectively, and τ_i is the isospin function fixed to be proton or neutron. The width parameter $\nu = 0.19 \text{ fm}^{-2}$ is used to minimize the ground state energy of ^{12}C . The AMD wave function is specified by a set of variational parameters, $\mathbf{Z} \equiv \{\mathbf{X}_1, \dots, \mathbf{X}_A, \xi_1, \dots, \xi_A\}$, which indicate Gaussian centroids and spin orientations of all single-particle wave functions.

In order to obtain the ground state wave function, the variation after angular-momentum and parity projections (VAP) for the 0^+ -projected AMD wave function is performed as

$$\frac{\delta}{\delta \mathbf{X}_i} \frac{\langle \Phi | H | \Phi \rangle}{\langle \Phi | \Phi \rangle} = 0, \quad (5)$$

$$\frac{\delta}{\delta \xi_i} \frac{\langle \Phi | H | \Phi \rangle}{\langle \Phi | \Phi \rangle} = 0, \quad (6)$$

$$\Phi = P_{MK}^{J\pi} \Phi_{\text{AMD}}(\mathbf{Z}), \quad (7)$$

where $P_{MK}^{J\pi}$ is the angular-momentum and parity projection operator. We denote the optimized parameter set \mathbf{Z} for the ground state as $\mathbf{Z}_{\text{VAP}}^0 = \{\mathbf{X}_1^0, \dots, \xi_1^0, \dots\}$.

To take into account 1p-1h excitations on the top of the obtained ground state, we consider small variation of

single-particle wave functions of $\Phi_{\text{AMD}}(\mathbf{Z}_{\text{VAP}}^0)$ by shifting the Gaussian centroid of the i th single-particle wave function, $\mathbf{X}_i^0 \rightarrow \mathbf{X}_i^0 + \epsilon \mathbf{e}_{\sigma}$, where ϵ is an enough small constant and \mathbf{e}_{σ} ($\sigma = 1, \dots, 8$) are unit vectors for 8 directions explained in Ref. [29]. As for the intrinsic spin of the shifted single-particle wave function, the spin non-flip and flip states are adopted. Consequently, totally $16A = 192$ wave functions of the spin non-flip and flip shifted AMD wave functions are superposed. We call this method, the shifted basis AMD (sAMD).

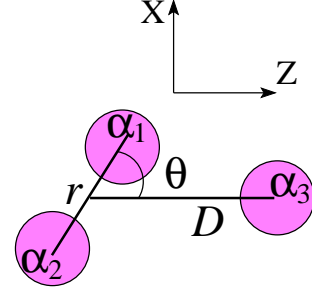


FIG. 1: (color online) Schematic figure of 3α configurations in the GCM for ^{12}C .

In addition to 1p-1h excitations expressed by the sAMD, we combine the GCM with the sAMD in order to take into account large amplitude dynamics of three α clusters by superposing various 3α configurations written by the Brink-Bloch cluster model wave functions [31]. Practically, a 3α -cluster configuration can be expressed with the AMD wave function by setting the parameters as $\mathbf{X}_i = \mathbf{S}_k$ for four nucleons ($p \uparrow$, $p \downarrow$, $n \uparrow$, and $n \downarrow$) in the k th α cluster (α_k). \mathbf{S}_k indicates the α_k cluster position and is given as

$$\mathbf{S}_1 = -\frac{1}{3}\mathbf{D} + \frac{\mathbf{r}}{2}, \quad (8)$$

$$\mathbf{S}_2 = -\frac{1}{3}\mathbf{D} - \frac{\mathbf{r}}{2}, \quad (9)$$

$$\mathbf{S}_3 = \frac{2}{3}\mathbf{D}. \quad (10)$$

Here the α_1 - α_2 and α_3 - $\alpha_1\alpha_2$ relative vectors, \mathbf{r} and \mathbf{D} , are chosen to be $\mathbf{r} = (r \cos \theta, r \sin \theta, 0)$ and $\mathbf{D} = (0, 0, D)$, respectively. θ is the angle between two vectors as shown in the schematic in Fig. 1. We use $r = \{0.8, 1.8, \dots, 4.8 \text{ fm}\}$, $D = \{1, 2, \dots, 7 \text{ fm}\}$, and $\theta = (\pi/8)i$ ($i = 0, \dots, 4$). Finally, in the sAMD+GCM, we superpose all the basis wave functions of the sAMD and 3α wave functions in addition to the original VAP wave function ($\Phi_{\text{AMD}}(\mathbf{Z}_{\text{VAP}}^0)$) as done in the previous work [29]. The final wave functions $\Psi(J_k^\pi)$ for the 0_k^+ and 1_k^- states are expressed by superposition of the J^π -projected wave functions with coefficients determined by diagonalizing the norm and Hamiltonian matrices.

In the sAMD+GCM method, the ground state is obtained by the VAP, and therefore, it already contains

the ground state correlation beyond mean-field approximation. In the sAMD, 1p-1h excitations on the ground state are taken into account by the linear combination of shifted Gaussian wave packets, and large amplitude cluster motion is treated by superposition of 3 α -cluster wave functions in the GCM. In the present method, the center of mass motion is exactly removed.

III. ISD OPERATORS AND TRANSITION STRENGTHS

In order to probe vorticity of the nuclear current, two kinds of operators have been used. One is the “toroidal mode” originally determined by the second order correction in the long-wave approximation of the transition $E\lambda$ operator in an electromagnetic field [10, 32], and the other is the “vortical mode” in Ravenhall-Wambach’s prescription [11]. Kvasil *et al.* described general treatment of toroidal, compressive, and vortical modes and their relation to each other [15]. They showed that the toroidal mode is a good probe for LE-ISD excitations rather than the vortical mode, though both the TD and vortical dipole (VD) operators can measure the vorticity. In this paper, we mainly discuss the TD and CD transitions. We also show the VD transitions just for comparison.

We use the TD, CD, and VD operators defined in Ref. [15] as

$$M_{\text{TD}}(\mu) = \frac{-i}{2\sqrt{3}c} \int d\mathbf{r} \mathbf{j}(\mathbf{r}) \times \left[\frac{\sqrt{2}}{5} r^2 \mathbf{Y}_{12\mu}(\hat{\mathbf{r}}) + r^2 \mathbf{Y}_{10\mu}(\hat{\mathbf{r}}) \right], \quad (11)$$

$$M_{\text{CD}}(\mu) = \frac{-i}{2\sqrt{3}c} \int d\mathbf{r} \mathbf{j}(\mathbf{r}) \times \left[\frac{2\sqrt{2}}{5} r^2 \mathbf{Y}_{12\mu}(\hat{\mathbf{r}}) - r^2 \mathbf{Y}_{10\mu}(\hat{\mathbf{r}}) \right], \quad (12)$$

$$M_{\text{VD}}(\mu) = \frac{-i}{2\sqrt{3}c} \int d\mathbf{r} \mathbf{j}(\mathbf{r}) \times \left[\frac{3\sqrt{2}}{5} r^2 \mathbf{Y}_{12\mu}(\hat{\mathbf{r}}) \right], \quad (13)$$

where $\mathbf{j}(\mathbf{r})$ is the current density operator and $\mathbf{Y}_{\lambda L\mu}$ is the vector spherical harmonics. Using the dipole operators we analyze the toroidal nature of the dipole excitations in the same matter as done in Ref. [33], which discussed dipole excitations of ^{10}Be . The detailed definition of $\mathbf{j}(\mathbf{r})$ as well as that of the density operator $\rho(\mathbf{r})$ is explained in appendix of Ref. [33]. For the current density, we take into account only the convection part of the nuclear current but omit its magnetization (spin) part. The matrix elements for the dipole transitions, $|0_1^+\rangle \rightarrow |1_k^-\rangle$, are given with the transition current

density $\delta\mathbf{j}(\mathbf{r}) \equiv \langle 1_k^- | \mathbf{j}(\mathbf{r}) | 0_1^+ \rangle$ as

$$\langle 1_k^- | M_{\text{TD}}(\mu) | 0_1^+ \rangle = \frac{-i}{2\sqrt{3}c} \int d\mathbf{r} \delta\mathbf{j}(\mathbf{r}) \left[\frac{\sqrt{2}}{5} r^2 \mathbf{Y}_{12\mu}(\hat{\mathbf{r}}) + r^2 \mathbf{Y}_{10\mu}(\hat{\mathbf{r}}) \right] \quad (14)$$

$$\langle 1_k^- | M_{\text{CD}}(\mu) | 0_1^+ \rangle = \frac{-i}{2\sqrt{3}c} \int d\mathbf{r} \delta\mathbf{j}(\mathbf{r}) \left[\frac{2\sqrt{2}}{5} r^2 \mathbf{Y}_{12\mu}(\hat{\mathbf{r}}) - r^2 \mathbf{Y}_{10\mu}(\hat{\mathbf{r}}) \right] \quad (15)$$

$$\langle 1_k^- | M_{\text{VD}}(\mu) | 0_1^+ \rangle = \frac{-i}{2\sqrt{3}c} \int d\mathbf{r} \delta\mathbf{j}(\mathbf{r}) \left[\frac{3\sqrt{2}}{5} r^2 \mathbf{Y}_{12\mu}(\hat{\mathbf{r}}) \right]. \quad (16)$$

Note that the CD matrix element can be transformed to the ordinary ISD matrix element (labeled IS1) by using the continuity equation $\nabla \cdot \mathbf{j} = -\frac{i}{\hbar} [H, \rho]$ as

$$\langle 1_k^- | M_{\text{CD}}(\mu) | 0_1^+ \rangle = \frac{E}{10\hbar c} \langle 1_k^- | M_{\text{IS1}}(\mu) | 0_1^+ \rangle, \quad (17)$$

$$M_{\text{IS1}}(\mu) \equiv \int d\mathbf{r} \rho(\mathbf{r}) r^3 Y_{1\mu}(\hat{\mathbf{r}}), \quad (18)$$

where E is the excitation energy of the 1_k^- .

For the 0_1^+ and 1_k^- wave functions obtained by the sAMD+GCM, we calculate the transition strengths of the dipole operators

$$\begin{aligned} & \tilde{B}(\text{TD, CD, VD}; 0_1^+ \rightarrow 1_k^-) \\ & \equiv \left(\frac{10\hbar c}{E} \right)^2 |\langle 1_k^- | M_{\text{TD, CD, VD}} | 0_1^+ \rangle|^2. \end{aligned} \quad (19)$$

Here we define the scaled transition strengths with the factor $\left(\frac{10\hbar c}{E}\right)^2$ so that $\tilde{B}(\text{CD})$ corresponds to the IS1 strength $B(\text{IS1}) = |\langle 1_k^- | M_{\text{IS1}} | 0_1^+ \rangle|^2$.

IV. RESULTS

A. Effective interactions

The adopted effective interactions are the same as those used in the previous work [29]. The central force is the MV1 force [34] consisting of two-range Gaussian two-body terms and a zero-range three-body term. As for the parametrization of the MV1 force, the case 1 with the Bartlett, Heisenberg, and Majorana parameters, $b = h = 0$ and $m = 0.62$, is used. In addition to the central force, the two-range Gaussian spin-orbit term of the G3RS force [35, 36] with the strengths $u_I = -u_{II} = 3000$ MeV is supplemented. This set of interaction parameters describes well properties of the ground and excited states of ^{10}Be and ^{12}C in the AMD+VAP calculations [37–39].

V. ISD EXCITATIONS OF ^{12}C OBTAINED WITH sAMD+GCM

We calculate the TD, CD, and VD transitions from the ground to 1^- states obtained by the sAMD+GCM. The calculated transition strengths are shown in Fig. 2 (a). The remarkable TD and VD strengths are obtained for LED states in the $E = 10 - 15$ MeV region, whereas the CD operator strengths are mainly distributed in the high-energy part corresponding to the ISGDR. The LE strengths are concentrated on two dipole states; one is the 1_1^- state at 12.6 MeV, which we assign to the experimental $1^-(10.844 \text{ MeV})$ state, and the other is the 1_2^- state at 14.8 MeV. The 1_2^- state has a significant 1p-1h component and approximately described within the sAMD model space. On the other hand, the 1_1^- state has a spatially developed 3α -cluster structure, which is a large amplitude cluster mode beyond the sAMD model space. It means that, in the 1^- spectra of ^{12}C , the large amplitude cluster mode exists in the energy lower than the 1p-1h dominant dipole excitation. The 3α -cluster structure of the 1_1^- state is consistent with the 3α -GCM calculation of Refs. [21, 22].

In order to see the significance of the large amplitude cluster motion in the LE-ISD excitations, we perform calculations within truncated model spaces by reducing 3α configurations. Figures 2(b), (c), and (d) show the ISD strengths obtained by the truncated calculations using the sAMD with $|\mathbf{S}_k| \leq 4 \text{ fm}$ 3α configurations, that with $|\mathbf{S}_k| \leq 3 \text{ fm}$, and the sAMD without 3α configurations, respectively. Note that $|\mathbf{S}_k|$ is the distance of the α_k -cluster center from the origin. In the calculations, the initial state is fixed to be the 0_1^+ state obtained by the full sAMD+GCM. As seen in Fig. 2(d), the sAMD without 3α configurations shows only one 1^- state in $E < 20$ MeV. The 1^- state has the dominant 1p-1h component with the remarkable TD strength, and approximately corresponds to the 1_2^- state of the full sAMD+GCM. In the sAMD result, there is no low-lying 3α -cluster state corresponding to the 1_1^- of the full sAMD+GCM. As 3α -cluster configurations are added to the sAMD model space, the 3α -cluster state appears around 20 MeV in the sAMD+GCM($|\mathbf{S}_k| \leq 3 \text{ fm}$) (Fig. 2(c)), comes down to 15 MeV in the sAMD+GCM($|\mathbf{S}_k| \leq 4 \text{ fm}$) (Fig. 2(b)), and finally becomes lower than the 1p-1h dominant 1_2^- state in the full sAMD+GCM. In other words, as the large amplitude inter-cluster motion develops, the cluster mode comes down to the lowest 1^- state crossing the 1p-1h state.

Figure 3 shows the energy-weighted sum (EWS) of the TD, VD, CD strengths up to $E = 20$ MeV obtained by the truncated and full calculations. The ratio to the total energy-weighted sum (TEWS_{full}) of the full sAMD+GCM is shown. The EWS value of the LE TD (VD) strengths is as much as 40 – 50% of the TEWS almost independently from the truncation of the 3α configurations. It means that the sum of the LE TD strengths is approximately described by the 1p-1h configurations

within the sAMD model space. As already shown in Figs. 2(a) and (d), the strength of the LE TD transition is originally concentrated at the single peak in the sAMD, and it is split into two LED states in the full sAMD+GCM as a result of coupling with the large amplitude 3α -cluster mode. By contrast, the LE CD transition strengths have only tiny percentages of the TEWS. The ratio is 2.5% in the sAMD, and it is raised up to 4 – 5% by 3α configurations. It means that about a half of the LE CD strengths is contributed by 1p-1h configurations and another half comes from 3α configurations.

Figure 4 shows comparison of the calculated IS1 strengths with the experimental data measured by α inelastic scattering. The calculated LE IS1 strengths are comparable to the experimental data. We assign the lowest peak for the calculated 1_1^- state to the experimental IS1 strength for the 1_1^- (10.84 MeV). The bump structure around $E = 15$ MeV in the experimental strength function is a candidate for the calculated 1_2^- state. In the present calculation, high-energy strengths for the ISGDR are distributed in the $E = 30 - 50$ MeV region more or less higher than the experimental ISGDR energy.

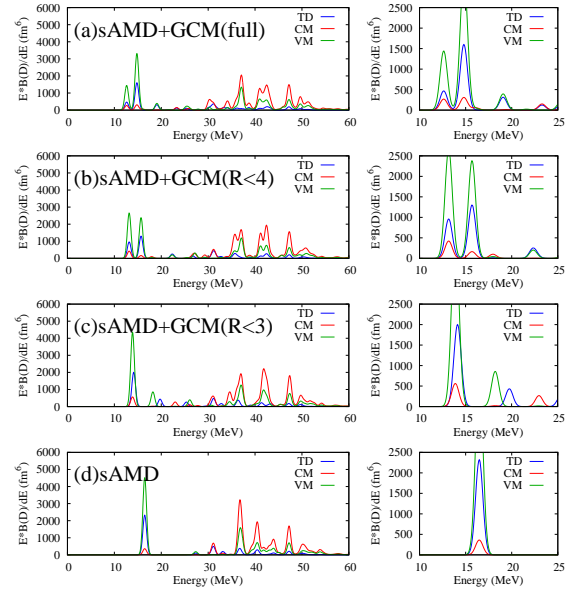


FIG. 2: (color online) The strength functions of the TD, CD, and VD transitions calculated with (a) the full sAMD+GCM, (b) sAMD with $|\mathbf{R}_k| \leq 4 \text{ fm}$ 3α configurations, (c) that with $|\mathbf{R}_k| \leq 3 \text{ fm}$ 3α configurations, and (d) sAMD without 3α configurations. The strengths of discrete states are smeared by Gaussian with the range $\gamma = 1/\sqrt{\pi} \text{ MeV}$.

VI. CLUSTER AND TOROIDAL NATURES OF THE LOW-ENERGY DIPOLE EXCITATIONS

In the present calculation, two LED modes are obtained in $E = 10 - 15$ MeV. One is the large-amplitude

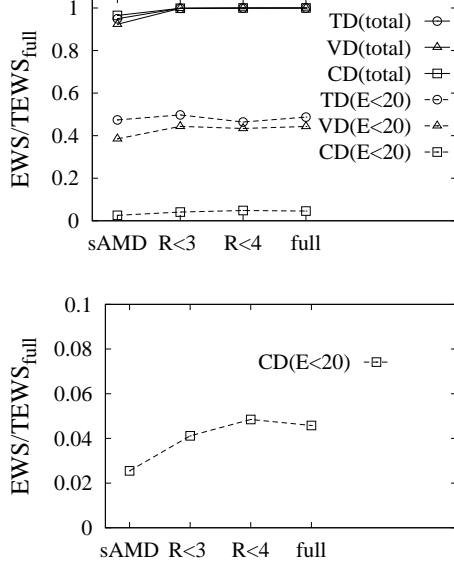


FIG. 3: Energy-weighted TD, VD, CD strengths summed up to $E = 20$ MeV obtained by the sAMD, sAMD+GCM ($|\mathbf{R}_k| \leq 3$ fm), sAMD+GCM ($|\mathbf{R}_k| \leq 4$ fm), and full sAMD+GCM calculations. The ratio to the total energy weighted sum ($TEWS_{full}$) value of the full sAMD+GCM is shown. The TEWS value of each calculation relative to the $TEWS_{full}$ is also shown.

3α -cluster mode, and the other is the 1p-1h dominant dipole excitation. We here discuss the cluster and toroidal natures of the LED states.

A. Occupation probabilities in shell-model expansion

Figure 5 shows the occupation probability of harmonic oscillator quanta N in the shell-model basis expansion with the size parameter $b = 1/\sqrt{2\nu}$. The dominant component of the 0_1^+ is the $0\hbar\omega$ configuration with 20% mixing of higher shell configurations. By contrast, the occupation probability of the 0_2^+ is distributed broadly in the high shell region because of the spatial developed 3α -cluster structure. Similarly to the 0_2^+ state, the 1_1^- state shows very broad distribution of the occupation probability due to the developed cluster structure. The 1_2^- state contains 40% $1\hbar\omega$ component indicating the dominant 1p-1h excitations with significant higher-shell mixing.

B. Intrinsic structures

In the sAMD+GCM calculation, each state is expressed by superposition of many different configurations of the shifted AMD and 3α wave functions. For intuitive understanding of the LED excitations, it is useful to con-

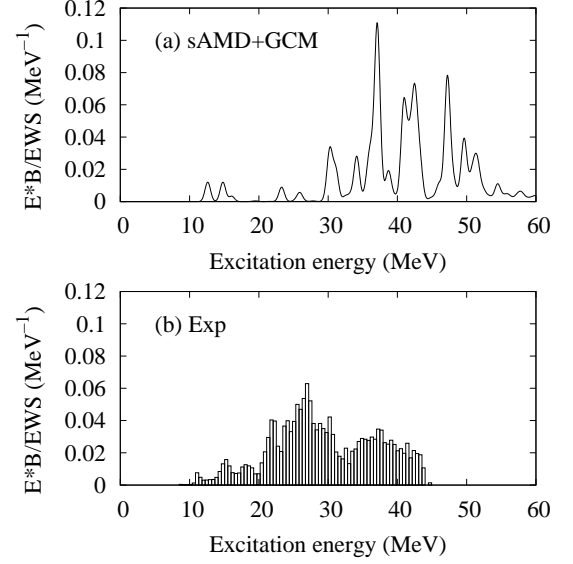


FIG. 4: The EWSR ratio of the energy weighted IS1 strengths. (a) The calculated strengths smeared by a Gaussian with the width $\gamma = 1/\sqrt{\pi}$ MeV. (b) The experimental data measured by α inelastic scattering from Ref. [18]. The figures are from Ref. [29].

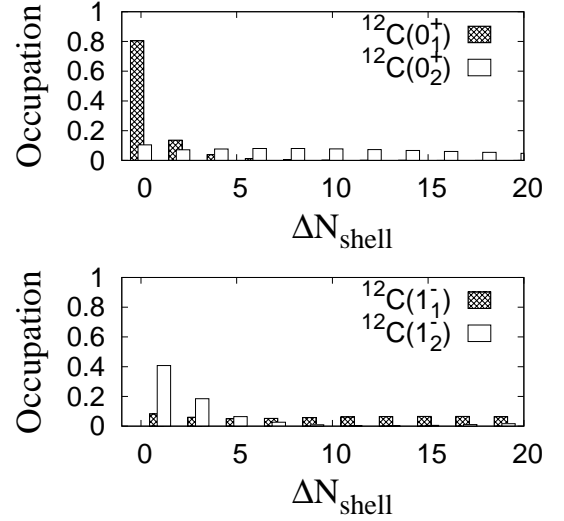


FIG. 5: Occupation probability of harmonic oscillator quanta N in the shell-model basis expansion of the $0_{1,2}^+$ and $1_{1,2}^-$ states obtained by the sAMD+GCM calculation. The horizontal axis indicates the difference ΔN from the minimum quanta $N_{min} = 8$.

sider a single Slater determinant which approximately describes the state of interest. We here perform simple model analysis by introducing model wave functions that have large overlap with the obtained 0_1^+ , 1_1^- , and 1_2^- states in order to discuss cluster and toroidal natures of

the LED modes in the intrinsic frame.

As for the model wave functions in the present analysis, we adopt an extended 3α (E- 3α) model based on the quasi α -cluster model proposed by Itagaki *et al.* [40], in which the α -breaking is taken into account by the cluster breaking parameter Λ . We start from the Brink-Bloch 3α -cluster wave functions, and incorporate the breaking of the twp α clusters, α_1 and α_2 .

Let us first consider the $\theta = \pi/2$ case for an isosceles triangle 3α configuration. An E- 3α wave function can be expressed by the AMD wave function with parameters

$$\mathbf{X}_i = \mathbf{S}_1 + i\mathbf{W}_i \quad (i = 1, \dots, 4), \quad (20)$$

$$\mathbf{X}_i = \mathbf{S}_2 + i\mathbf{W}_i \quad (i = 5, \dots, 8), \quad (21)$$

$$\mathbf{X}_i = \mathbf{S}_3 \quad (i = 9, \dots, 12), \quad (22)$$

$$\mathbf{W}_i = \Lambda \left(\mathbf{e}_{\sigma i} \times \frac{\mathbf{r}}{2} \right) \quad (i = 1, \dots, 4), \quad (23)$$

$$\mathbf{W}_i = \Lambda \left(\mathbf{e}_{\sigma i} \times \left(-\frac{\mathbf{r}}{2} \right) \right) \quad (i = 5, \dots, 8). \quad (24)$$

The spin and isospin functions are fixed to be $\tau_i \chi_i = p \uparrow, p \downarrow, n \uparrow, n \downarrow$ for $i = \{1, 5, 9\}, i = \{2, 6, 10\}, i = \{3, 7, 11\}, i = \{4, 8, 12\}$, respectively, and $\mathbf{e}_{\sigma i}$ indicates the unit vector for the spin orientation. Λ describes the α -breaking because of the spin-orbit interaction through the imaginary part \mathbf{W}_i of the Gaussian centroid \mathbf{X}_i , which depends on the intrinsic spin orientation. In the $\Lambda > 0$ case, \mathbf{W}_i indicates finite momenta of nucleons boosted by the spin-orbit potential. In the $\Lambda = 0$ case, the E- 3α wave function becomes equivalent to the ideal Brink-Bloch 3α -cluster wave function without the α -breaking. Next, a non-isosceles triangle 3α configuration is constructed by rotating the α_1 and α_2 clusters with the angle $\pi/2 - \theta$ around $-\mathbf{D}/3$. Consequently, an E- 3α wave function used here is specified by parameters, r, D, θ , and Λ . We denote the E- 3α wave function $\Phi_{\text{E-}3\alpha}(r, D, \theta, \Lambda)$, which is expressed by a single Slater determinant.

We search for the E- 3α wave functions that have large overlap with the obtained $0_1^+, 1_1^-,$ and 1_2^- states and regard them as dominant configurations of the corresponding states. The intrinsic density distributions of the dominant configurations for the $0_1^+, 1_1^-$, and 1_2^- states are shown in Fig. 6. The 0_1^+ state has 85% overlap with the 0^+ -projected $\Phi_{\text{E-}3\alpha}$ with $r = 1$ fm, $D = 2$ fm, $\theta = \pi/2$, and $\Lambda = 0.5$ corresponding to a compact isosceles triangle structure with the significant α -breaking component. The E- 3α wave function has almost the consistent structure with the AMD wave function obtained by the VAP for the 0_1^+ . The 1_1^- state has 60% overlap with the BB-cluster 3α wave function with $r = 5.8$ fm, $D = 5$ fm, and $\theta = \pi/4$ projected onto the $J^\pi K = 1^-1$ state, indicating the spatially developed 3α structure. The 1_2^- state is the toroidal mode originally obtained as the 1_1^- state in the sAMD calculation. It has large overlap with $\Phi_{\text{E-}3\alpha}$ with $r = 1$ fm, $D = 2$ fm, $\theta = 3\pi/8$, and $\Lambda = 0.5$ projected onto $J^\pi K = 1^-1$ state, and corresponds to the compact triangle configuration with the cluster breaking. It has 75% overlap with the 1p-1h dominant TD mode of the sAMD. For the 1_2^- state of the sAMD+GCM, the

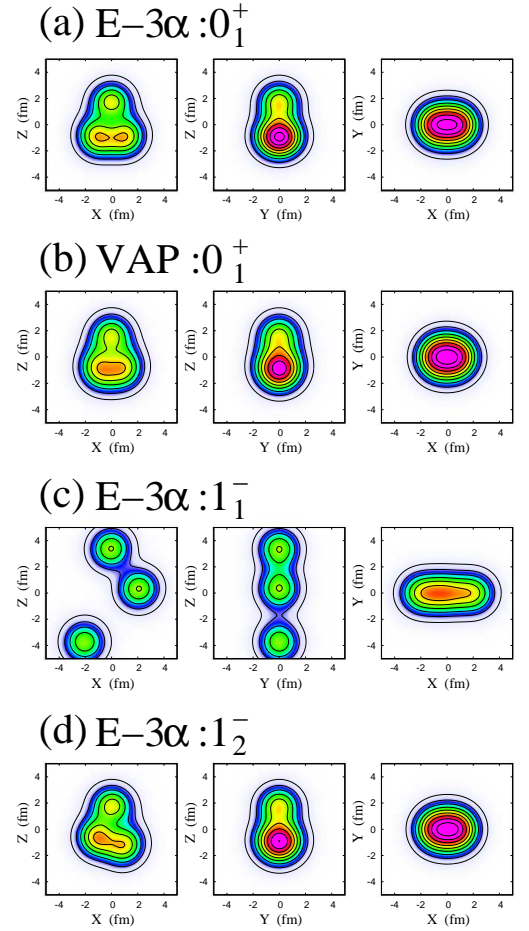


FIG. 6: (color online) Intrinsic density distributions of the dominant configurations written by the E- 3α wave functions for (a) the 0_1^+ , (c) 1_1^- , and (d) 1_2^- states. The intrinsic density of the AMD wave function $\Phi_{\text{AMD}}(\mathbf{Z}_{\text{VAP}}^0)$ obtained by the VAP for the ground state is also shown.

overlap is reduced to be 50% because of the coupling with the large-amplitude 3α -cluster mode. As shown in Fig. 6, the dominant configuration of the TD mode for the 1_2^- state shows the intrinsic structure similar to that for the 0_1^+ state except for the slight rotation (tilting) of the 2α part.

Figure 7 shows the transition current density for the transition between the dominant configurations of the 0_1^+ and 1_2^- . The transition current density from the positive-parity projected initial state to the negative-parity projected final state is shown in Fig. 7(a). The intrinsic densities without the parity projection of the initial and final configurations are shown again in Figs. 7(b) and (c). The transition current density clearly shows the toroidal nuclear current with the $K = 1$ feature in the prolately deformed intrinsic system, and describes the remarkable TD strengths for the $0_1^+ \rightarrow 1_2^-$ transition. In a cluster picture, the toroidal current is understood by the rotation of the 2α subsystem as shown in a schematic figure

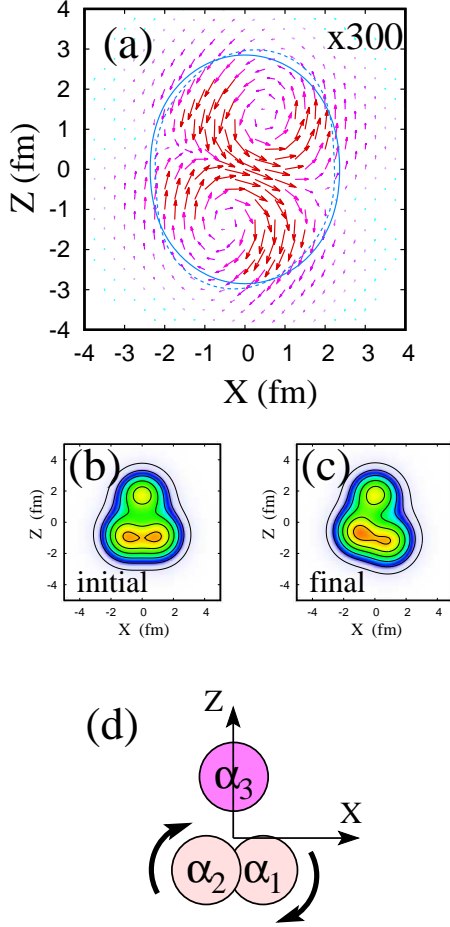


FIG. 7: (color online) (a) Transition current density for $0_1^+ \rightarrow 1_2^-$ in the intrinsic frame (at $Y = 0$ on the X - Z plane). The vector plot of the transition current density for the parity-projected states of the dominant E-3 α configurations is shown. Red solid and magenta dashed lines indicate contours for the matter densities $\rho(X, 0, Z) = 0.08 \text{ fm}^{-3}$ of the parity-projected initial and final states, respectively. (b) Intrinsic density distributions of the dominant configuration for the initial state (0_1^+) and (c) that of the final state (1_2^-). (d) Schematic figure for the $0_1^+ \rightarrow 1_2^-$ excitation in the cluster picture. α_1 and α_2 clusters contain the cluster breaking.

of Fig. 7(d). It means that the 2 α -cluster rotation induces the TD dominant dipole excitation. Note that the 2 α subsystem in the initial and final states consists of not ideal α clusters but somewhat dissociated ones expressed by the α -breaking parameter $\Lambda = 0.5$ as mentioned previously.

Similar mechanism was found in ^{10}Be as discussed in Ref. [33]. In the case of ^{10}Be , the system is approximately understood by the $^6\text{He} + \alpha$ clustering, and the TD

dominant dipole excitation in the 1_1^- state is described by rotation of the ^6He cluster. An interesting difference from ^{10}Be is that the large-amplitude cluster mode exists below the TD mode in the dipole excitations of ^{12}C .

C. TD mode in shell-model limit

As discussed previously, the TD mode can be understood as the rotational excitation of the 2 α subsystem. Instead of the cluster picture, it is worth to discuss features of the TD mode in terms of 1p-1h excitations. Indeed, the 1_2^- contains 40% $1\hbar\omega$ component as the dominant configuration, though it has significant mixing of higher shell components because of the coupling with the 3 α -cluster state. We here consider 1p-1h representation of the TD mode by taking a shell-model limit of the E-3 α wave functions for the dominant configurations.

As explained previously, the ground state is approximately described by $\Phi_{\text{E-3}\alpha}$ with $r = 1 \text{ fm}$, $D = 2 \text{ fm}$, $\theta = \pi/2$, $\Lambda = 0.5$ projected onto the $J^\pi = 0^+$ state, whereas the dominant component of the TD mode is described by $\Phi_{\text{E-3}\alpha}$ with $r = 1 \text{ fm}$, $D = 2 \text{ fm}$, $\theta = 3\pi/8$, $\Lambda = 0.5$ projected onto the $J^\pi K = 1^-1$ state. By taking the limit of $\sqrt{\nu}r \ll 1$ and $\sqrt{\nu}D \ll 1$, we can map the dominant configurations to $0\hbar$ and $1\hbar\omega$ configurations in the shell-model limit for the ground state and the TD mode, respectively. For simplicity, we discuss the shell-model limit of the K^π -projected configuration in the intrinsic frame.

The shell-model limit of the E-3 α wave function is represented by four-nucleon (4N: two protons and two neutrons) configurations around the SU(3)-limit 2 α core with the $|000\rangle^4|001\rangle^4$ configuration. Here $|n_x n_y n_z\rangle$ means the single-particle state in the harmonic oscillator potential with the size parameter $b = 1/\sqrt{2\nu}$. For single-particle states around the $|000\rangle^4|001\rangle^4$ core, we use the following notations,

$$|p_{+\frac{3}{2}}\rangle = \frac{1}{\sqrt{2}}(|100\rangle + i|010\rangle)|\uparrow\rangle, \quad (25)$$

$$|p_{+\frac{1}{2}}\rangle = \frac{1}{\sqrt{2}}(|100\rangle + i|010\rangle)|\downarrow\rangle, \quad (26)$$

$$|p_{-\frac{1}{2}}\rangle = \frac{1}{\sqrt{2}}(|100\rangle - i|010\rangle)|\uparrow\rangle, \quad (27)$$

$$|p_{-\frac{3}{2}}\rangle = \frac{1}{\sqrt{2}}(|100\rangle - i|010\rangle)|\downarrow\rangle, \quad (28)$$

$$|sd_{+\frac{1}{2}}\rangle = |002\rangle|\uparrow\rangle, \quad (29)$$

$$|sd_{-\frac{1}{2}}\rangle = |002\rangle|\downarrow\rangle. \quad (30)$$

For the $K^\pi = 0^+$ - and $K^\pi = 0^-$ -projected states of the ground state and the TD mode, the 4N configurations in the shell-model limit are written as

$$\begin{aligned}
P_{K=0}^+ \Phi_{4N}(\text{g.s.}) &= \lambda_+^4 |p_{+\frac{3}{2}} p_{-\frac{3}{2}} p_{+\frac{3}{2}} p_{-\frac{3}{2}}\rangle |ppnn\rangle \\
&+ \lambda_+^2 \lambda_-^2 |p_{+\frac{3}{2}} p_{-\frac{3}{2}} p_{+\frac{1}{2}} p_{-\frac{1}{2}}\rangle (|ppnn\rangle + |nnpp\rangle + |pnnp\rangle + |nppn\rangle) \\
&+ \lambda_-^4 |p_{+\frac{1}{2}} p_{-\frac{1}{2}} p_{+\frac{1}{2}} p_{-\frac{1}{2}}\rangle |ppnn\rangle,
\end{aligned} \tag{31}$$

$$\begin{aligned}
P_{K=1}^- \Phi_{4N}(\text{TD}) &= \lambda_+^4 \left(|p_{+\frac{3}{2}} sd_{-\frac{1}{2}} p_{+\frac{3}{2}} p_{-\frac{3}{2}}\rangle + |p_{+\frac{3}{2}} p_{-\frac{3}{2}} p_{+\frac{3}{2}} sd_{-\frac{1}{2}}\rangle \right) |ppnn\rangle \\
&+ \lambda_+^2 \lambda_-^2 \left(|p_{+\frac{3}{2}} sd_{-\frac{1}{2}} p_{+\frac{1}{2}} p_{-\frac{1}{2}}\rangle + |p_{+\frac{3}{2}} p_{-\frac{3}{2}} p_{+\frac{1}{2}} sd_{+\frac{1}{2}}\rangle \right) (|ppnn\rangle + |nnpp\rangle + |pnnp\rangle + |nppn\rangle) \\
&+ \lambda_-^4 \left(|p_{+\frac{1}{2}} sd_{+\frac{1}{2}} p_{+\frac{1}{2}} p_{-\frac{1}{2}}\rangle + |p_{+\frac{1}{2}} p_{-\frac{1}{2}} p_{+\frac{1}{2}} sd_{+\frac{1}{2}}\rangle \right) |ppnn\rangle,
\end{aligned} \tag{32}$$

where $\lambda_+ : \lambda_- = (1 + \Lambda) : (1 - \Lambda)$. For simplicity, we here assume $r/\sqrt{\nu} \ll D/\sqrt{\nu} \ll 1$ and an enough small θ to omit spin-flip excitations. It is shown that the shell-model limit for the ground state is not a simple paring state but linear combination of correlating nn , pp , and np pairs in $p_{+3/2}p_{-3/2}$ and $p_{+1/2}p_{-1/2}$. Spin and isospin configurations are strongly correlated with each other because of the α -like correlation. The coefficients of the $p_{+3/2}p_{-3/2}p_{+3/2}p_{-3/2}$, $p_{+3/2}p_{-3/2}p_{+3/2}p_{-3/2}$, and $p_{+1/2}p_{-1/2}p_{+1/2}p_{-1/2}$ terms are determined by the α -breaking parameter Λ . The $\Lambda = 1$ case corresponds to the uncorrelated $4N$ state with the pure $p_{+3/2}p_{-3/2}p_{+3/2}p_{-3/2}$ configuration around the 2α core. The TD mode is expressed by 1p-1h excitations of $p_{-3/2}^{-1}sd_{-1/2}$ and $p_{-1/2}^{-1}sd_{+1/2}$ on the top of the ground state configuration. They are coherent 1p-1h excitations changing the oscillator quanta $n_\perp \equiv n_x + n_y$ and n_z as $\Delta n_\perp = -1$ and $\Delta n_z = +2$, and contribute to the remarkably strong TD transition.

VII. SUMMARY AND OUTLOOK

We have investigated cluster and toroidal natures of the ISD excitations in ^{12}C based on the sAMD+GCM calculation. In the $E = 10 - 15$ MeV region, we have found two LED modes. One is the spatially developed 3α -cluster state and the other is the TD mode. The TD mode is dominantly described by coherent 1p-1h excitations on the ground state. The cluster state comes down to the energy lower than the TD mode because of the large amplitude cluster motion.

For the CD (ordinary ISD) excitations, the transition strengths are mainly distributed in the high-energy re-

gion for the ISGDR, whereas 5% of the TEWS exist in $E < 20$ MeV consistently to the experimental data. In the experimental data of the CD strengths, the bump structure at $E \sim 15$ MeV is a candidate for the 1_2^- state of the 1p-1h dominant TD mode. The LED states are strongly excited by the TD operator. In the present calculation, two modes, the cluster and TD modes, are coupled with each other. As a result of the coupling, the TD strengths for the 1_1^- and 1_2^- states are the same order. Unfortunately, there is no established method to experimentally observe the TD strengths.

We have discussed the feature of the TD mode from the cluster picture based on the model analysis by analyzing dominant configurations in the single-Slater expression. In the analysis, the transition current density clearly shows the toroidal nature of the TD mode induced by the rotation of the 2α -like deformed subsystem. We have also discussed the connection of the rotational excitation of the cluster with 1p-1h excitations by taking the shell-model limit of the dominant configurations. The TD mode can be understood as the coherent 1p-1h excitations on the ground state, in which spin and isospin configurations are highly correlated because of the α -type four-body correlation.

Acknowledgments

The computational calculations of this work were performed by using the supercomputer in the Yukawa Institute for theoretical physics, Kyoto University. This work was supported by JSPS KAKENHI Grant Nos. 26400270 and 16J05659.

-
- [1] T. Yamada, Y. Funaki, T. Myo, H. Horiuchi, K. Ikeda, G. Ropke, P. Schuck and A. Tohsaki, Phys. Rev. C **85**, 034315 (2012).
 - [2] Y. Chiba, M. Kimura and Y. Taniguchi, Phys. Rev. C **93**, 034319 (2016).
 - [3] N. Paar, D. Vretenar, E. Khan and G. Colo, Rept. Prog.

- Phys. **70**, 691 (2007).
- [4] T. Aumann and T. Nakamura, Phys. Scr. **T152**, 014012 (2013).
- [5] D. Savran, T. Aumann and A. Zilges, Prog. Part. Nucl. Phys. **70**, 210 (2013).
- [6] A. Bracco, F. C. L. Crespi and E. G. Lanza, Eur. Phys.

- J. A **51**, 99 (2015).
- [7] M. N. Harakeh and A. E. L. Dieperink, Phys. Rev. C **23**, 2329 (1981).
 - [8] P. Decowski, H. P. Morsch and W. Benenson, Phys. Lett. **101B**, 147 (1981).
 - [9] T. D. Poelheken, S. K. B. Hesmondhalgh, H. J. Hofmann, A. van der Woude and M. N. Harakeh, Phys. Lett. B **278**, 423 (1992).
 - [10] S. F. Semenko, Sov. J. Nucl. Phys. **34**, 356 (1981).
 - [11] D. G. Ravenhall and J. Wambach, Nucl. Phys. A **475**, 468 (1987).
 - [12] D. Vretenar, N. Paar, P. Ring, and T. Nikšić Phys. Rev. C **65**, 021301 (2002).
 - [13] N. Ryezayeva *et al.*, Phys. Rev. Lett. **89**, 272502 (2002).
 - [14] P. Papakonstantinou, V. Y. Ponomarev, R. Roth and J. Wambach, Eur. Phys. J. A **47**, 14 (2011).
 - [15] J. Kvasil, V. O. Nesterenko, W. Kleinig, P.-G. Reinhard and P. Vesely, Phys. Rev. C **84**, 034303 (2011).
 - [16] A. Repko, P.-G. Reinhard, V. O. Nesterenko and J. Kvasil, Phys. Rev. C **87**, 024305 (2013).
 - [17] V. O. Nesterenko, J. Kvasil, A. Repko, W. Kleinig and P.-G. Reinhard, Phys. Atom. Nucl. **79**, 842 (2016).
 - [18] B. John, Y. Tokimoto, Y.-W. Lui, H. L. Clark, X. Chen and D. H. Youngblood, Phys. Rev. C **68**, 014305 (2003).
 - [19] Y. Fukushima and M. Kamimura, *Proc. Int. Conf. on Nuclear Structure, Tokyo, 1977, edited by T. Marumori* J. Phys. Soc. Jpn. **44**, 225 (1978).
 - [20] M. Kamimura, Nucl. Phys. **A351**, 456 (1981).
 - [21] E. Uegaki, S. Okabe, Y. Abe and H. Tanaka, Prog. Theor. Phys. **57**, 1262 (1977).
 - [22] E. Uegaki, Y. Abe, S. Okabe and H. Tanaka, Prog. Theor. Phys. **62**, 1621 (1979).
 - [23] Y. Kanada-En'yo, H. Horiuchi and A. Ono, Phys. Rev. C **52**, 628 (1995).
 - [24] Y. Kanada-En'yo and H. Horiuchi, Phys. Rev. C **52**, 647 (1995).
 - [25] Y. Kanada-En'yo and H. Horiuchi, Prog. Theor. Phys. Suppl. **142**, 205 (2001).
 - [26] Y. Kanada-En'yo, M. Kimura and A. Ono, PTEP **2012**, 01A202 (2012).
 - [27] Y. Kanada-En'yo, Phys. Rev. C **89**, 024302 (2014).
 - [28] Y. Kanada-En'yo, Phys. Rev. C **93**, 024322 (2016).
 - [29] Y. Kanada-En'yo, Phys. Rev. C **93**, 054307 (2016).
 - [30] M. Kimura, Phys. Rev. C **95**, no. 3, 034331 (2017).
 - [31] D. M. Brink, *Proc. Int. School of Physics Enrico Fermi, Course 36*, Varenna, ed. C. Bloch (Academic Press, New York, 1966).
 - [32] V.M. Dubovik and A.A. Cheshkov, Sov. J. Part. Nucl. **5**, 318 (1975).
 - [33] Y. Kanada-En'yo and Y. Shikata, Phys. Rev. C **95**, no. 6, 064319 (2017) doi:10.1103/PhysRevC.95.064319 [arXiv:1704.05649 [nucl-th]].
 - [34] T. Ando, K. Ikeda, and A. Tohsaki, Prog. Theor. Phys. **64**, 1608 (1980).
 - [35] R. Tamagaki, Prog. Theor. Phys. **39**, 91 (1968).
 - [36] N. Yamaguchi, T. Kasahara, S. Nagata, and Y. Akaishi, Prog. Theor. Phys. **62**, 1018 (1979).
 - [37] Y. Kanada-En'yo, Phys. Rev. Lett. **81**, 5291 (1998).
 - [38] Y. Kanada-En'yo, H. Horiuchi and A. Dote, Phys. Rev. C **60**, 064304 (1999).
 - [39] Y. Kanada-En'yo, Prog. Theor. Phys. **117**, 655 (2007) [Prog. Theor. Phys. **121**, 895 (2009)].
 - [40] N. Itagaki, H. Masui, M. Ito and S. Aoyama, Phys. Rev. C **71**, 064307 (2005).